SAND2015-8414 R
LDRD PROJECT NUMBER: 123456
LDRD PROJECT TITLE: Development of a MEMS dual-axis differential capacitance floating element shear stress sensor
PROJECT TEAM MEMBERS: Casey Barnard, Benjamin Griffin

ABSTRACT: (250 word limit)
A single-axis MEMS wall shear stress sensor with differential capacitive transduction method is produced. Using a synchronous modulation and demodulation interface circuit, the system is capable of making real time measurements of both mean and fluctuating wall shear stress. A sensitivity of 3.44 mV/Pa is achieved, with linearity in response demonstrated up to testing limit of 2 Pa. Minimum detectable signals of 340 μPa at 100 Hz and 120 μPa at 1 kHz are indicated, with a resonance of 3.5 kHz. Multiple full scale wind tunnel tests are performed, producing spectral measurements of turbulent boundary layers in wind speeds ranging up to 0.5 Ma (18 Pa of mean wall shear stress). The compact packaging allows for minimally invasive installation, and has proven relatively robust over multiple testing events. Temperature sensitivity, likely due to poor CTE matching of packaged materials, is an ongoing concern being addressed. These successes are being directly leveraged into a development plan for a dual-axis wall shear stress sensor, capable of producing true vector estimates at the wall.

INTRODUCTION:
Direct measurement of wall shear stress at the small scales required for full resolution of relevant perturbations within a turbulent boundary layer has been an open problem for many decades now. Quantification of wall shear stress could enable the design of more drag efficient vehicles, be used in active flow feedback control regimes, and improve the fundamental understanding of fluid dynamics within complex three-dimensional flow fields.

Indirect methods of wall shear stress estimation exist, but suffer from a number of inherent drawbacks. They all rely on extensive calibration in-situ, limiting their flexibility to a small subset of testing applications. Even then measurements are not made of wall shear stress, but some other metric (velocity, thermal transfer, etc), and must be correlated to a wall shear stress estimate via modeling, which always carries additional error.

Force balances and floating element devices have been used for some time, however none of them have been tailored to the unique requirements of a low speed aerodynamic flow. To fully resolve the dynamics of the turbulent structures as they interact with the wall, it is necessary to obtain sufficient bandwidth with a small sensing element. Specifically, using the inner wall length scales as a reference, the sensing element dimensions should be smaller than 20y+ with a bandwidth greater than 1/3t+. At a flow speed of 40 m/s, with a Reynolds number of 2500, this corresponds to a 200 μm element size and a bandwidth of 47 kHz for full resolution. Additionally, within a turbulent boundary layer the pressure forces are typically three orders of magnitude stronger than the wall shear stress forces. Thus, cross axis rejection is a very important design parameter. Changing environmental conditions, namely relative humidity and temperature, must also be accounted for.

The advent of MEMS provided a window towards a possible solution, with micro-machined floating element wall shear stress sensors first being developed in 1988. High surface area to volume ratios inherent to MEMS devices leads to favorable scaling. Pressure gradient and alignment errors are reduced from monolithic wafer integration and tightly controlled dimensions afforded by modern fabrication techniques.

Numerous transduction methods have been implemented, most importantly optical, piezoresistive, and capacitive. As reported in the literature, optical methods have been limited by a need for visual access, external light sources, or strong cross axis sensitivities to vibration. Piezoresistive sensors exhibit high levels of temperature sensitivity and associated thermal drift. A recurring difficulty for all transduction types is the ability to simultaneously measure mean and fluctuating changes in wall shear stress (DC and AC signal components).
Recent efforts utilizing capacitive transduction have leveraged the work done in the communications industry, implementing an amplitude modulation scheme for simultaneous measurements. This work should be viewed as a continuation of those efforts, addressing short comings in packaging and reliability that limited the overall effectiveness of the sensor. Improvements to circuit architecture also result in a reduced noise floor and long term stability, while maintaining the same order of sensitivity. Once refinements of the single-axis design are completed, novel efforts will be made towards developing the first dual-axis micro-fabricated wall shear stress sensor.

DETAILED DESCRIPTION OF EXPERIMENT/METHOD:

Device design is based on previous iterations of MEMS floating element wall shear stress sensors, with a set of interdigitated comb fingers. As wall shear stress is generated on the device die by a passing fluid, the floating element will be displaced. A set of four tethers, in an H-bar configuration, acts as the restoring springs. Element displacement also changes the distance between the comb fingers, acting as a pair of variable gap capacitors with three distinct electrodes, where the center one is shared, as seen in Figure 1. Thickness of the supporting tethers is kept much larger than their width, to reduce sensitivity to orthogonal pressure inputs. The differential orientation of the interdigitated comb fingers provides added sensitivity to in-plane shear, while also ideally rejecting common mode inputs.

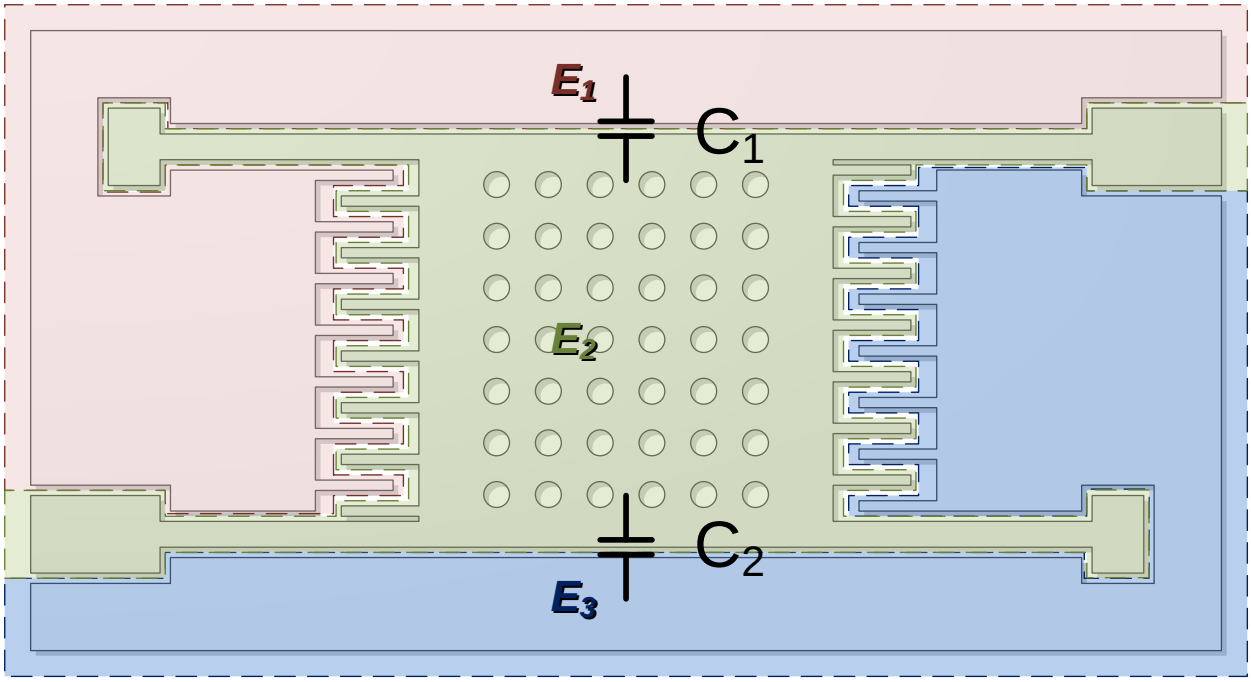

Figure 1: Schematic of CSSS floating element structure, separated into three electrodes forming two capacitive gaps.

Quasi-static analysis provides a deflection estimate for a given force, with electrostatic analysis providing output voltage estimates for a given deflection. The most significant source of signal attenuation is the "secondary" gap, formed between adjacent sets of fingers separated by smaller "primary" gaps. Increasing the number of finger pairs increases overall nominal capacitance of the primary gap structure, but also decreases the distance to the secondary gaps, increasing their parasitic contribution. Two modes of dynamic device performance are constructed with lumped element modeling techniques, for both wall shear stress and pressure.

Optimization of the device design is carried out with a descending gradient sequential quadratic programming algorithm (MATLAB's fmincon function). Minimum detectable signal is chosen as the minimization objective function. Non-linear constraints are implemented on non-linear deflection components of deflection, resonance of the physical structure, and bias voltages to avoid electrostatic pull-in. All physical dimensions are also bound limited. Initial starting values are randomly generated within the bounds, and the algorithm ran numerous times, to maximize the probability that the locally optimized result is sitting in a global design space minima. The key design variable governing mechanical performance is tether width, which is minimized (to maximized compliance, and thus sensitivity) while maintaining the target resonance of 5 kHz.

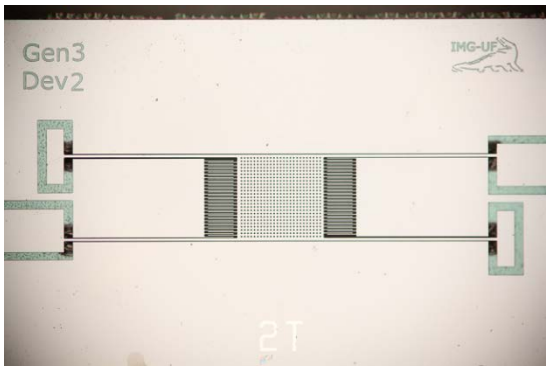

Figure 2: microscope image capture of fabricated CSSS structure.

MEMS die are bulk-machined in silicon substrates with a 6-mask process. Wafers with integrated poly-silicon through silicon vias (TSVs) are sourced externally from IceMOS Technologies, with a buried oxide layer of 1.5 µm between a 50 µm device layer (with Phosphorous doping targeting a resistivity below 0.02 Ohms-cm) and a 400 µm handle. Aluminum/Silicon contact pads are patterned on both sides of the device. A protective nitride layer is coated over the backside for electrical and environmental isolation. Thermal annealing is performed until the TSV to contact pad junctions are Ohmic, as measured by a HP4510A semiconductor parameter analyzer. Two DRIE steps define the device layer structure and a large open back cavity for device release. Figure 2 shows a fully fabricated and released device. Die level electrostatic actuation tests are performed to select operational devices for packaging.

Hydraulic smoothness of the device frontside is necessary to avoid disturbing boundary layer dynamics. Roughness under a limit of 5 y+ is considered hydraulically smooth, which for 20 m/s flow over a flat plate corresponds to 50 µm. Typical wirebonds extend over 100 µm above the surface of the sensor. To obviate these concerns devices with integrated through silicon vias (TSVs) are produced, which moves the electrical connection internal to the package housing. A laser machined plastic shim cap fits around the silicon die, producing a flush front surface when inset into a recessed steel tube. Currently displayed measurements and results still use a frontside wirebond approach for electronic connections (see Figure 3), as TSV packaging methodology is still under development.

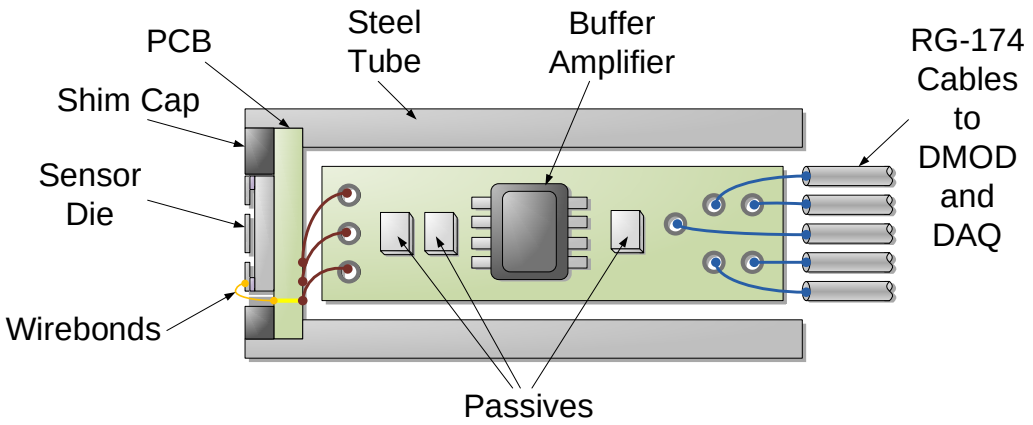

Figure 3: CSSS packaging with frontside wirebonds.

To enable DC measurements with a capacitive transduction method, specialized interface circuitry is developed. Output impedance of the device is measured around 10-20 pF, including the capacitive gaps (~5 pF) and electrical interconnects (wirebond or TSV). To reduce signal degradation associated with such a high output impedance, a unity gain voltage buffer is co-located within the packaged sensor head. A synchronous modulation-demodulation support circuit provides sinusoidal biases to the two electrodes, 180 degrees out of phase with each other. Independent tuning of the bias magnitudes allows for balancing of the physically realized sensor to have nominally zero sinusoidal output. The carrier frequency used is 1 MHz, which transfers the AC component of the signal up, reducing the impact of low frequency interference and noise. Changes in DC wall shear stress input are reflected in increasing the sinusoidal carrier component, where the direction of input determines the polarity of the shift. A phase locked timing signal ensures proper demodulation and rectification, with a low pass filter eliminating residual carrier components. The system is then capable of providing solely baseband signal content, containing both fluctuating and mean wall shear stress components, in real time.

RESULTS:

Characterization of device performance is achieved with a number of testing facilities, at both tabletop and full scale levels. Electrical performance is evaluated with two metrics: noise floor over frequencies of interest and drift in DC offset. At 100 Hz the noise floor is 1200 nV/rt(Hz), as measured by a Stanford Research Systems SR560 dynamic signal analyzer set to 800 FFT lines over a range of 800 Hz, with results shown in Figure 4. Drift is below 0.2 mV/hr, as measured with a Keithley 2000 digital multimeter with measurement range of +/- 1 V and averaging intervals of 10 PLC.

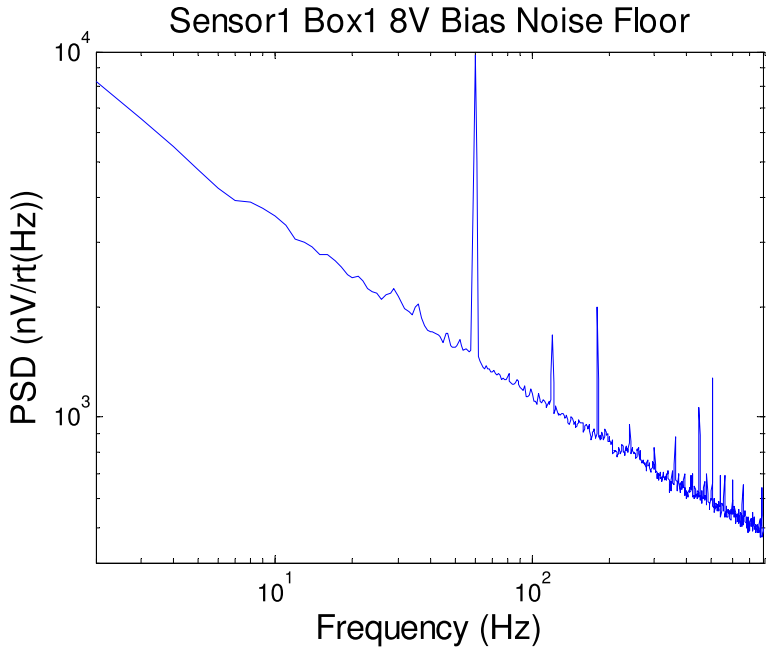

Figure 4: noise floor of the CSSS with synch MOD-DMOD system.

Response to changes in ambient environmental conditions is evaluated with a ESPEC environmental control chamber. The DC offset of the system is measured over a range of humidity and temperature conditions, ranging from 40 to 80 percent relative humidity and 15 to 35 C. Results are displayed in Figure 5. Changes in RH lead to relatively small output differences, effectively less than 1 Pa of error. Temperature was a more significant factor, leading to an effective 5 Pa of shift when held at the higher RH.

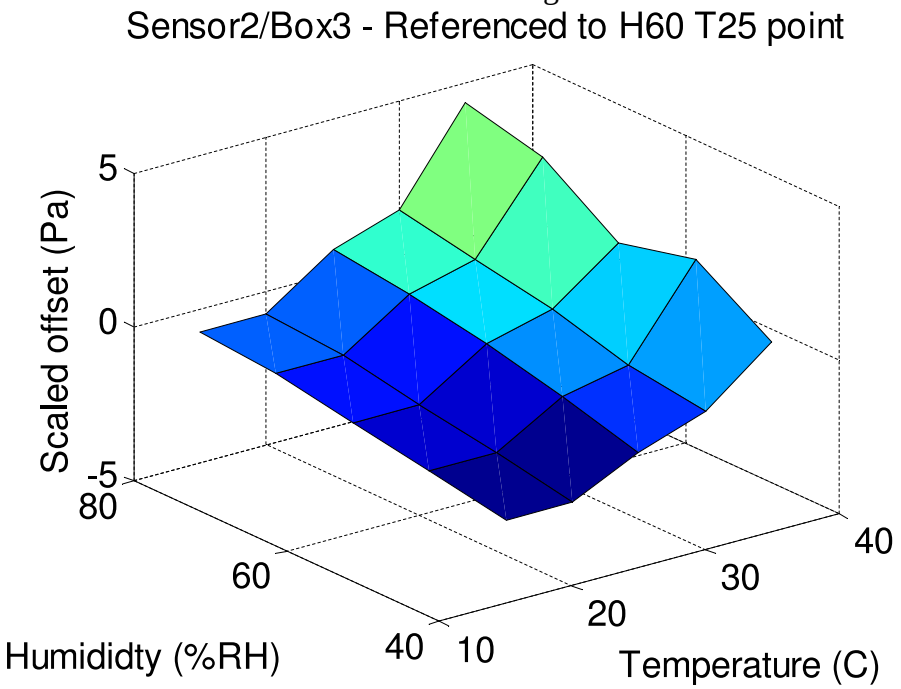

Figure 5: DC offset of CSSS system under different environmental conditions.

Sensitivity to DC shear is measured with a laminar flow cell, which uses the Poiseulle flow model of pressure driven flow to estimate shear at the wall given a linear pressure gradient, measured via a set of taps. Response is linear up to 1.8 Pa, the limits of the testing platform, giving a sensitivity of 3.44 mV/Pa, as seen in Figure 6.

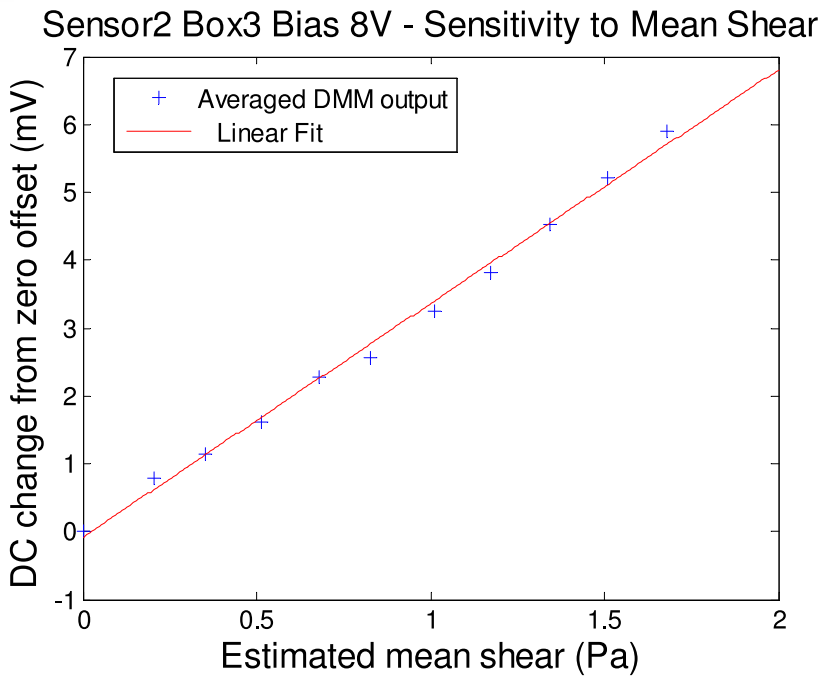

Figure 6: CSSS system sensitivity to mean wall shear stress inside flow cell testing rig.

Directional measurement capabilities are also validated within the flow cell by performing ramp measurements in various rotational orientations of the sensor. Seen in Figure 7, a 180 rotation yields a near-mirror image, and gives the same sensitivity.

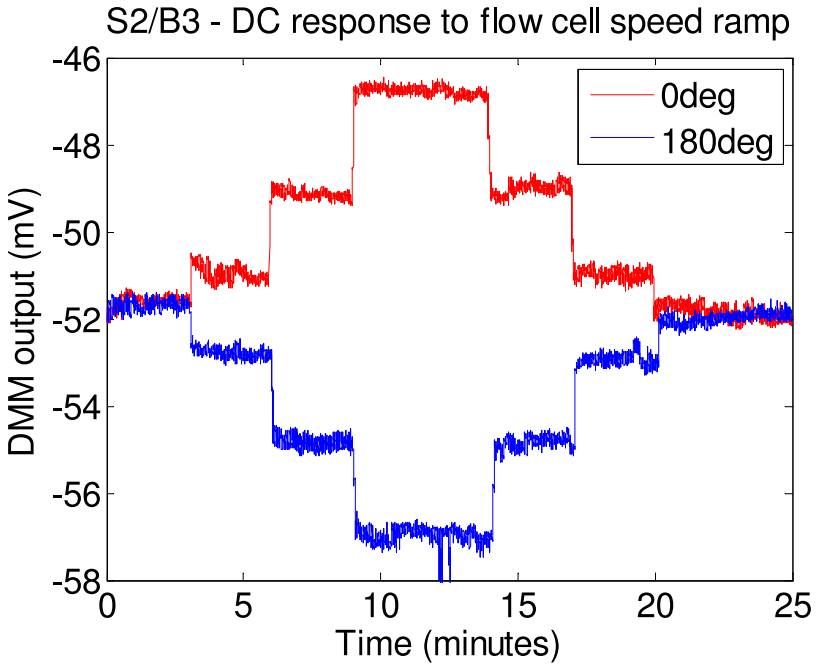

Figure 7: display of directional sensing from CSSS system. The device is subjected to mean wall shear stress inside the flow cell at varying flow speeds. The sensor is then rotated, such that flow is passing over in the opposite direction, and test is repeated.

Sensitivity to AC shear is measured with an acoustic plane wave tube, which uses the Stokes layer excitation of near wall particles in acoustic standing waves to provide a known fluctuating shear input. The PWT is driven at 1,128 Hz with acoustic termination pressure ranging from 80 to 160 dB in 5 dB steps. This corresponds to 2 Pa of shear stress at the maximum level. Fluctuating wall shear stress sensitivity is calculated as 3.45 mV/Pa, shown in Figure 8.

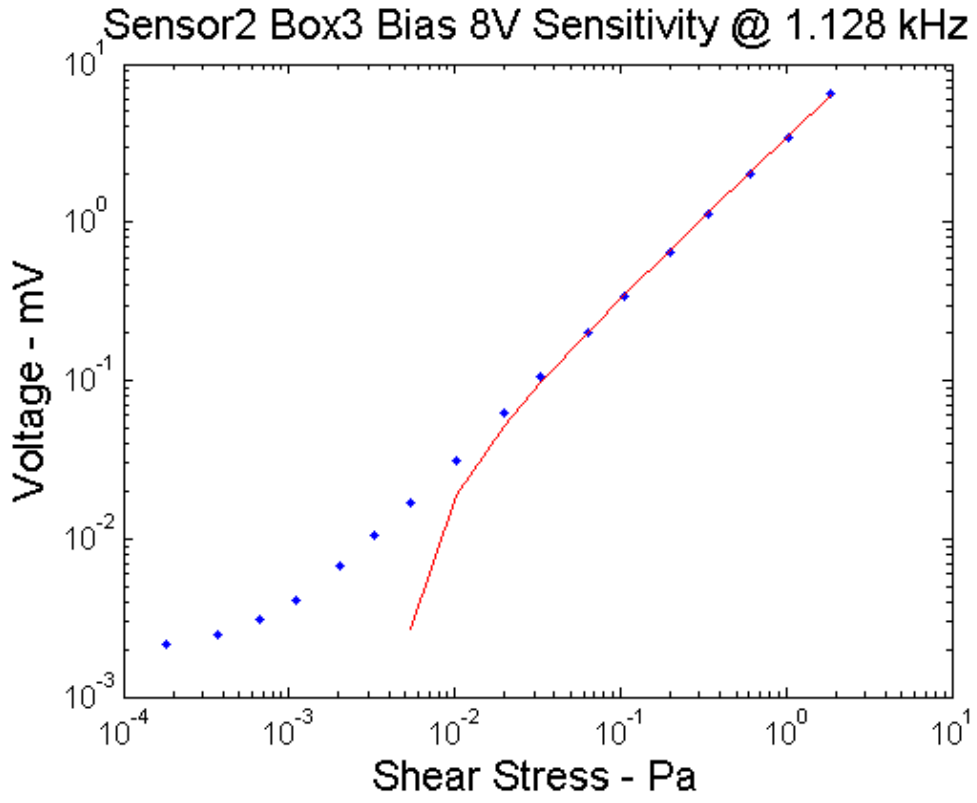

Figure 8: CSSS system sensitivity to fluctuating wall shear stress in acoustic plane wave tube testing rig.

To determine the frequency response function of the device a modified PWT is used. Installation of a variable position hard wall termination allows for positioning of the CSSS at the pressure minima, velocity maxima location of the standing wave pattern for a range of frequencies. Figure 9 displays results of measurements made from 200 to 4,000 Hz reveal a sensor resonance typically around 3,000 to 3,500 Hz, with a usable flat band (as defined by a +/- 3 dB standard) of 2,000 Hz.

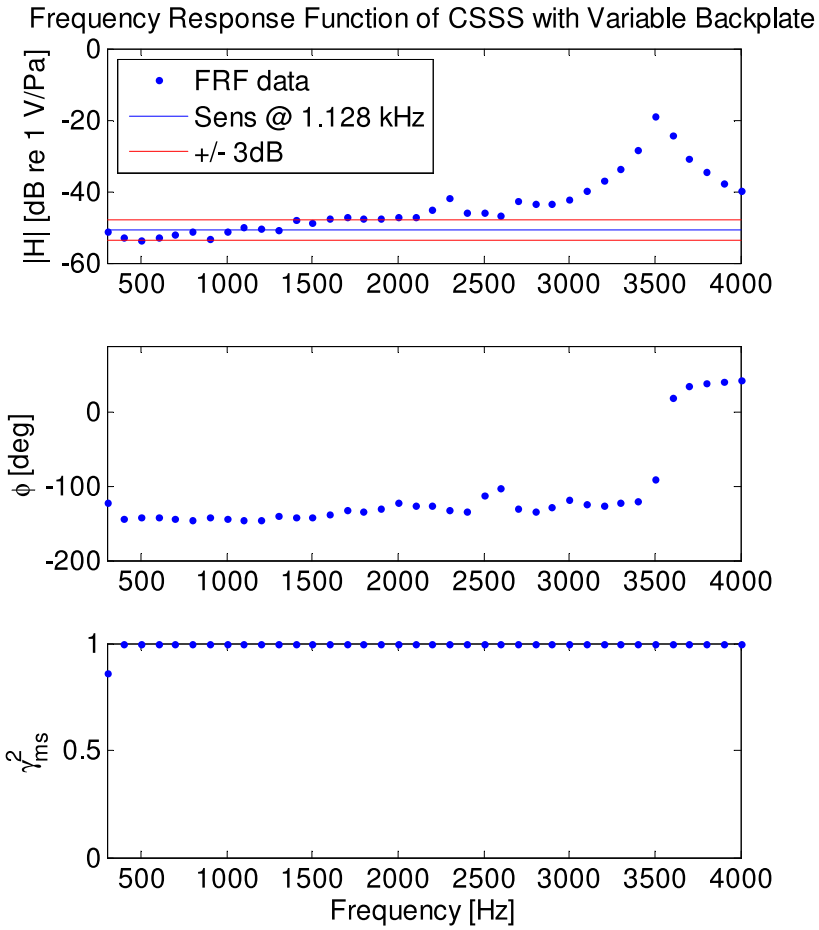

Figure 9: frequency response function of CSSS system. Measured inside the acoustic plane wave tube with a movable hard wall termination, to keep the sensor at a pressure node for all tested frequencies.

Senisitivity to dynamic pressure is measured with the CSSS inset at the tube termination, and is calculated as 0.98 µV/Pa, corresponding to a pressure rejection ratio of over 71 dB at 1,128 Hz. Figure 10 displays these results.

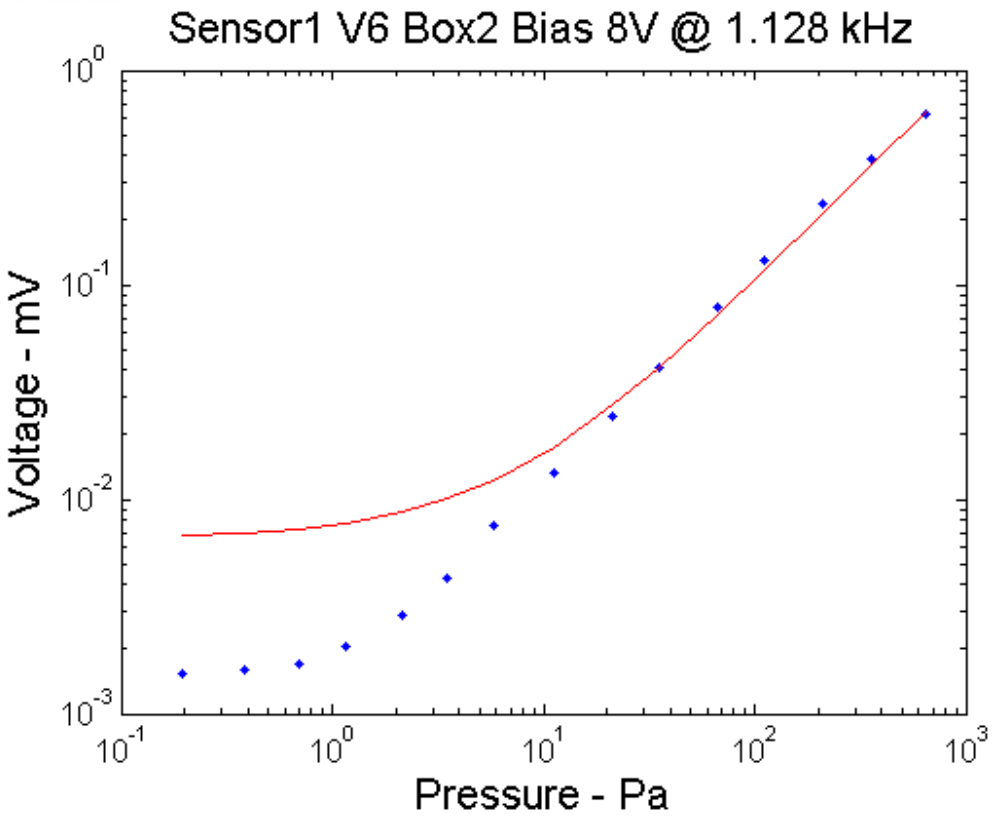

Figure 10: CSSS system sensitivity to normal incident pressure waves tested inside the acoustic plane wave tube.

Full scale testing efforts are initiated at the University of Florida ELD model closed loop low-speed flow facility. A zero pressure gradient flat plate model is installed within the test section. Velocities are varied from 0 to 30 m/s. A traversing hotwire capable of independent three axis movement is used as a comparative measurement tool. Analysis of the AC spectra (Figure 11) reveals the transition of the turbulent boundary layer from laminar to turbulent. The relatively low sensor resonance limits the data collection efforts, but the beginning of a roll-off in the spectra typically expected in turbulent boundary layers is clear.

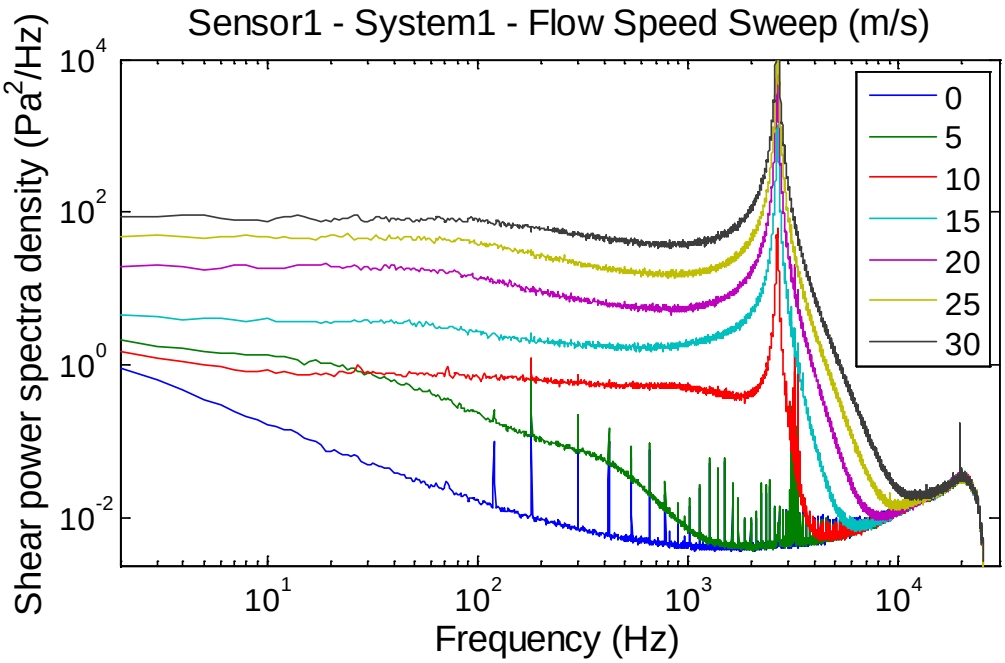

Figure 11: PSD of CSSS system response inside closed loop wind tunnel with ZPG flat plate model at University of Florida. Flow speeds are varied from 0 to 30 m/s in 5 m/s intervals.

Similar results are seen at the first external facility, the California Institute of Technology, also in an ELD model closed loop low-speed tunnel with ZPG flat plate model. Rotation of the CSSS 180 degrees shows stability of response in both orientations, once settled, seen in Figure 12. Note, the color represents a given flow speeds, where the two lines of a given color are the test results in both rotational positions. At 28 m/s the measured mean wall shear stress is roughly 0.9 Pa.

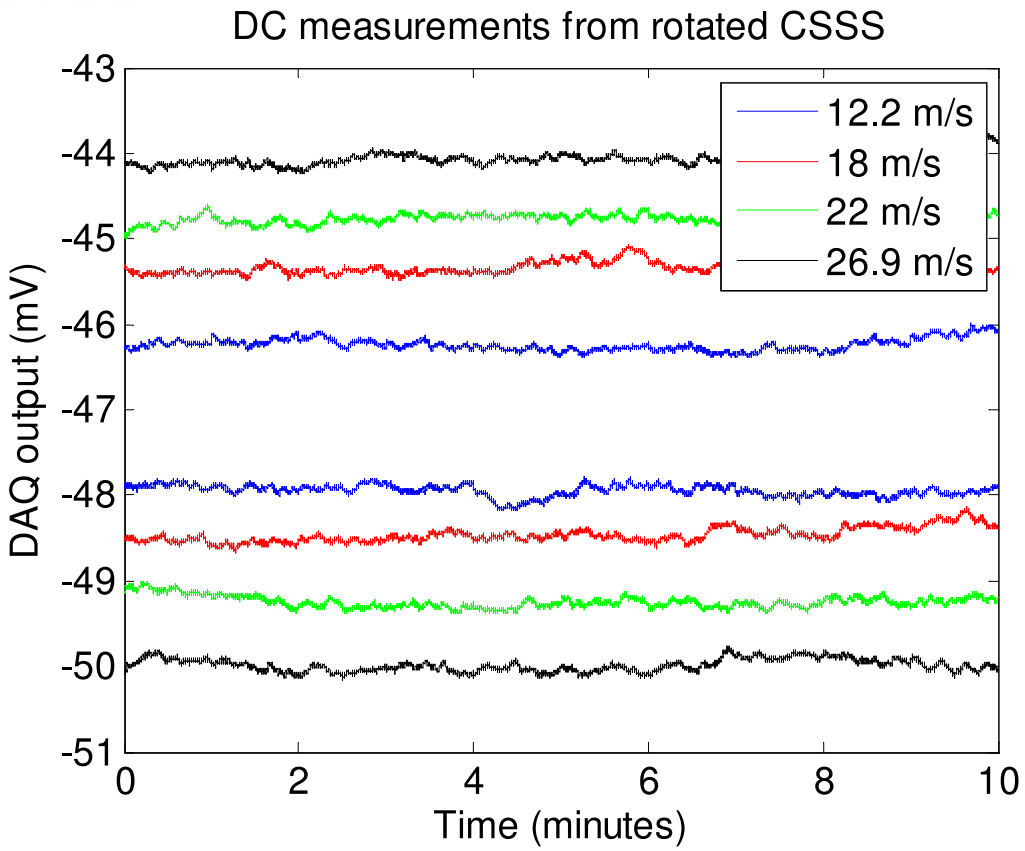

Figure 12: measurement of DC output from CSSS system at varying flow speeds inside CalTech closed loop tunnel facility. The sensor is allowed to settle at all speeds, showing in-test stability. Rotation of sensor shows similar response.

A second set of external tests is performed at the NASA Langley Research Center Curved Duct Test Rig, typically used for testing of acoustic liners and impedance eduction efforts. The CSSS is installed in the duct wall, with both hard wall and acoustic liner conditions. Fan driven flow speed is varied from 0 to 0.5 Ma, with acoustic excitation profiles of single tone plane waves and broadband. DC response from the system is displayed in Figure 13. While this corresponds to over 18 Pa of mean wall shear stress, there is very little hysteresis in sensor response. Spectral analysis shows negligible difference in fluctuating wall shear stress measurements between the wall conditions.

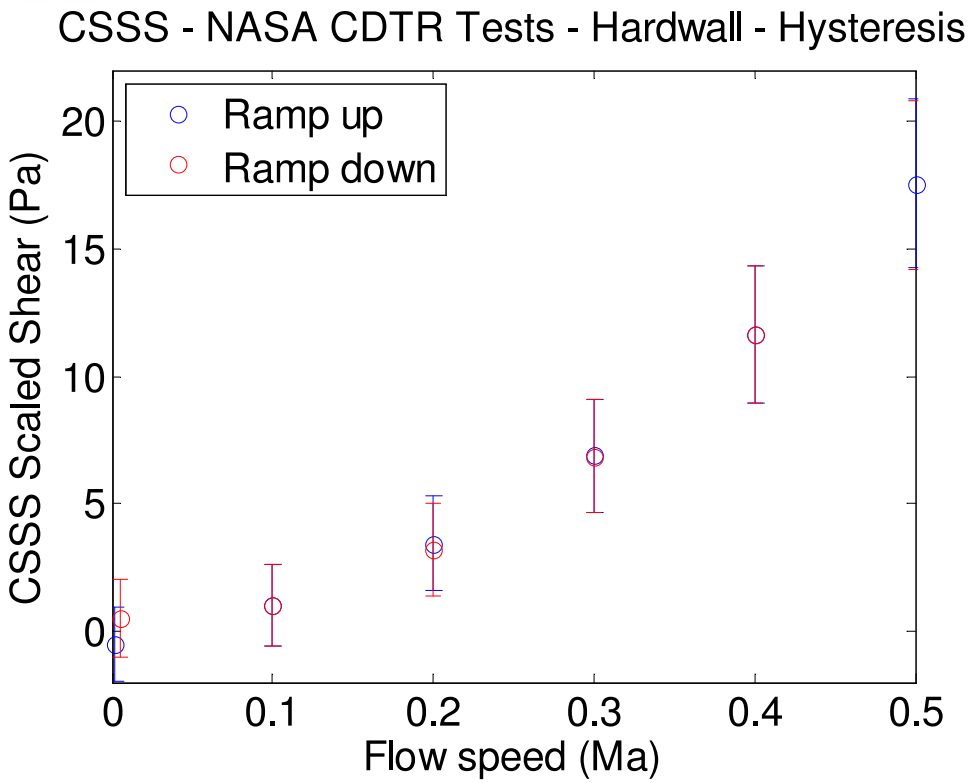

Figure 13: hysteresis measurement of CSSS system DC response inside closed duct test rig at NASA LaRC.

DISCUSSION:

This is the first reported MEMS wall shear stress sensor to survive multiple full scale tests at different locations, producing measurements of wall shear stress within the turbulent boundary layer of low to moderate speed wind tunnels. Minimum detectable signal, calculated at 340 μPa at 100 Hz, is among the lowest ever reported.

The largest source of error seen thus far is from changes in ambient testing conditions. In the case of the NASA LaRC CDTR test, where tunnel inlet air is drawn from outdoors, there is very little control over temperature and relative humidity. As this technology continues to transfer from prototype to useable tool, it will be subjected to further environmental exposure and abuse. For example, an upcoming test at NASA LaRC will make use of their 20'x14' closed loop facility, which uses ¼ scale plane models and can reach temperatures well over 100 F during Summer testing, providing a daunting test of sensor robustness.

It is speculated that poor coefficient of thermal expansion (CTE) matching within the packaging cap is the primary culprit of temperature sensitivity. Silicon typically has a CTE of around 3 ppm, where the FR4 circuit board it is adhered to has a CTE of around 20 ppm. By changing the substrate to a laminated stack of woven Kevlar combined with a low CTE epoxy resin, printed circuit board (PCB) substrates as low as 6 ppm can be specially constructed. Attachment of the silicon die to the PCB can also be modified, moving away from the thermally cured (150 C for 2

hours) epoxy film used currently. Using an epoxy that cures at a lower temperature, or even at room temperature, would help to minimize residual stress acting on the MEMS.

Another source of possible error is the electrostatic environment directly surrounding the sensor. At the CalTech facilities, when the tunnel is turned on or off, the DC response has two distinct components to it, displayed in Figure 14. The first is a relatively abrupt shift in output, which correlates to the change in mean tunnel velocity and hence mean wall shear stress. The second is a much longer rolling behavior, consistent with RC charging or discharging. Similar behavior can be observed in the UF ELD tunnel. It is postulated that triboelectric charging of the flat plate model, which is made of insulating acrylic, is generating an electrostatic field that alters the mean operating condition of the sensor system. A different research group, working on arrays of capacitive wall shear stress sensors, has observed a similar phenomenon. Covering the insulating plate with a metallic paint, and then providing a ground line, eliminated the effect.

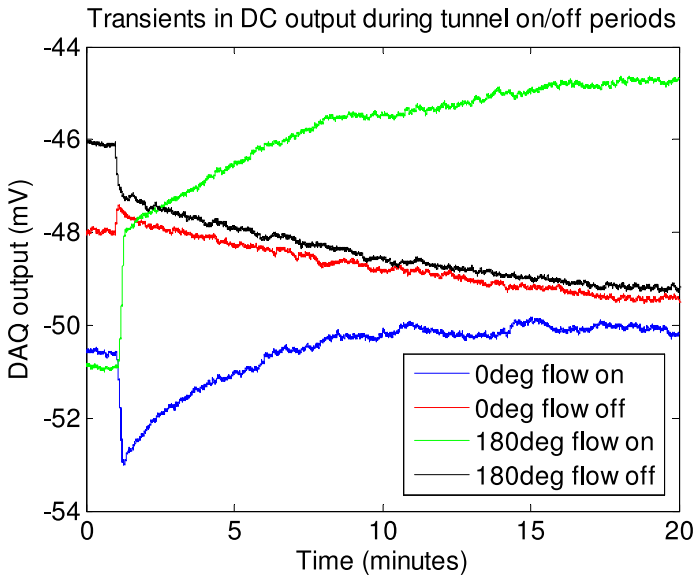

Figure 14: transients in CSSS system DC response when wind tunnel power turned on or off. It is theorized to be an effect of electrostatic charging on the acrylic plate.

Full uncertainty analysis estimates still need to be performed. For frequency response function estimates, the position of the sensor at the pressure node is essential. With a moveable back plate currently controlled by a stepper motor, the step interval can be relatively large at the higher frequencies. When using hotwires as comparative measurements and performing correlation analysis, there is a finite phase offset between the measurement systems which needs quantification. A recently completed relative phase delay plane wave tube rig is undergoing characterization. Mean flow is introduced to the tube to simulate the general operating environment seen inside the tunnel, with an acoustic wave driven on top acting as a deterministic event to sample. Completion of this setup will lead to more accurate comparisons between velocity and wall shear stress fields.

Integration of TSVs requires slight changes to the standard sensor cap assembly as well. Moving the contact pads to the backside of the die, and internal to the steel tube, can be achieved in a

number of ways. Wirebonding to the backside through a milled access port, followed by encapsulation of the wirebond pad junctions with conductive epoxy and silicone RTV for protection. Once the shim cap is attached, and the assembly inserted into the tube end, a scanning white light interferometer is used to validate front side flushness. There remains concern over flushness during installation, as the most common method for introducing a sensor is with an interface holder which sets the relative sensor position with a set screw. Typically this is done by eye, but even if a purpose made assembly rig is constructed it will still be limited by machining tolerances. At +/- 5 mil finish, there is still over 100 μm of uncertainty, well beyond the flushness limit at the smallest scales.

ANTICIPATED IMPACT:

A few minor refinements are required to finish development of the single-axis wall shear stress sensor designs, and move them into a state easily accessible to the external user. A large part of that is in packaging, which in its current state suffers from a lack of proper strain relief. Using a three part packaging approach (a possible schematic is seen in Figure 15), with hard contact joints between the different segments, would greatly reduce this problem. Additionally it would allow for easier debugging or repairs, as only the affected portion could be replaced independently.

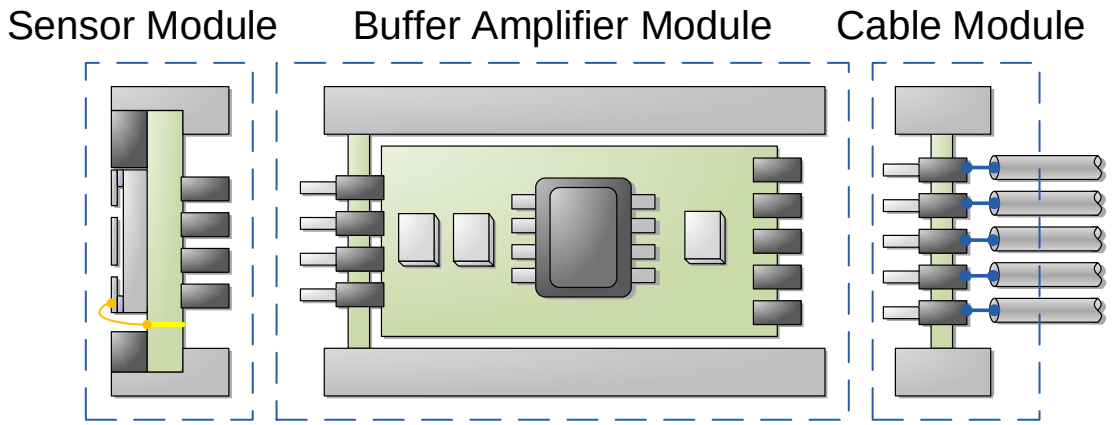

Figure 15: packaging concept for modular three part design.

Full resolution of spatial and temporal scales still remains as an issue. MEMS die with smaller floating elements, and stiffer tethers for a higher bandwidth, have been fabricated already, but not yet packaged. Their robustness requires further verification. However the design and optimization approach used here could be tailored to different applications, targeting the bandwidth and size they require.

Continued improvements aside, these testing results for single-axis devices are indicative of the viability of both the general approach and particular implementation of this wall shear stress sensor system. Within a few years it is expected this technology will be commercially available, enabling exterior groups to further explore complex flow fields. Cost may remain prohibitively

high for some, as the small market size for purely experimental aerodynamic instrumentation does not lend itself to mass production.

These results for single-axis performance, coupled with early modeling and simulations, point to the viability of capacitive MEMS as a suitable methodology for true vector wall shear stress measurement. As proposed, the general development plan would remain largely the same, with small modifications to the production steps along the way.

Selection of appropriate tethers is the most difficult question at this juncture. The design of multi-axis accelerometers is leveraged to find the support structure which maximizes both directions of in-plane deflection, while minimizing orthogonal response. Two sets of interdigitated comb fingers are situated on all four sides of the floating element, forming four distinct capacitors. A possible design schematic is displayed in Figure 16.

Once tether designs have been selected and optimized, the fabrication process continues with the exact same mask set as before. Changing the layout of the frontside DRIE step is the only predicted change. Test structures on previous wafers, with serpentine and crab leg flexures, indicated no issues. Further packaging development only requires the addition of two more contact points to either end of the buffer amplifier board, to pass the second bias set.

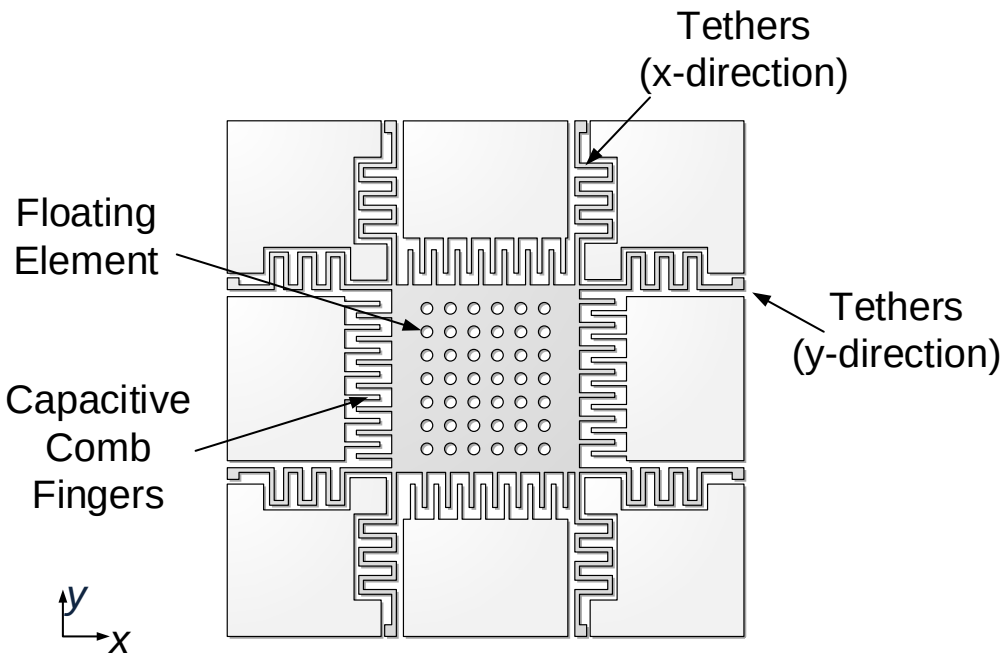

Figure 16: possible schematic for dual-axis CSSS.

Because the four capacitors share a single central electrode, the interface electronics needs to be split and replicated. Treating each directional axis as independent, two separate sets of phase locked bias signals are used. Keeping the carrier signals sufficiently far away from each other, such that the baseband information does not overlap, allows for effective isolation of the two axes. Carrier signals are kept close enough to avoid overlapping harmonics, with frequencies of 1

and 1.2 MHz initially used. Demodulation of the combined signal at either of the two phase locked timing switches returns the baseband information for the associated axis. Simulations of this approach indicate no cross-talk or distortion of response level, whether the baseband signal tones are shared or distinct. Figure 17 shows the spectra of two signals, each composed of 3 distinct sinusoids with different power levels, that have been passed through the simulation at different modulation frequencies.

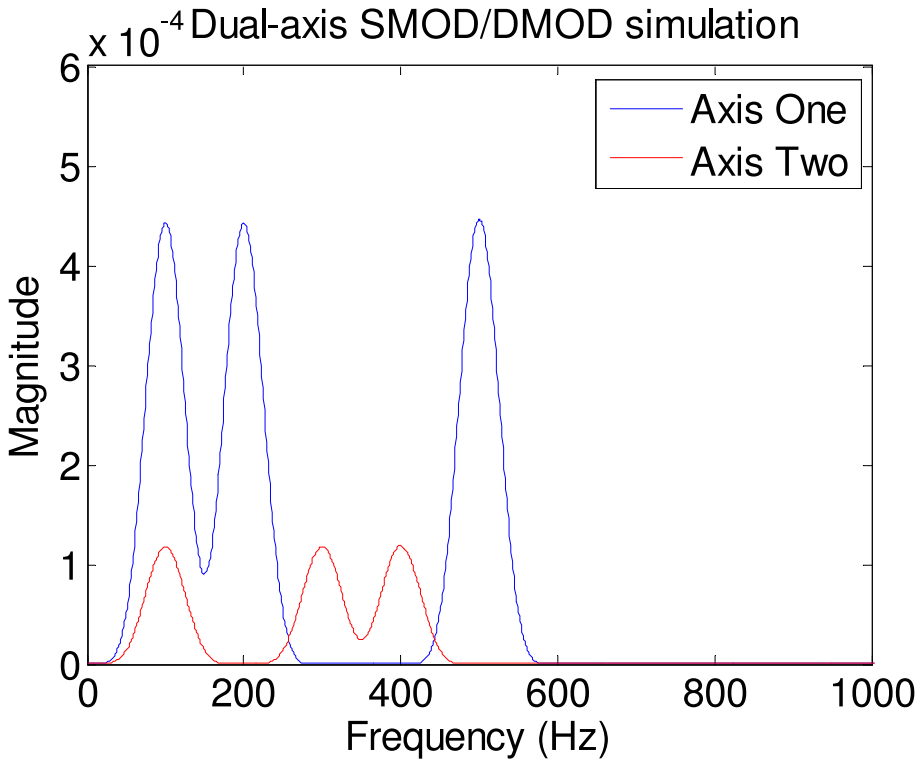

Figure 17: simulation result of dual-axis CSSS system with two isolated modulation frequencies. There is no distortion of signal between modulated axes.

Characterization and testing is carried out in a multi-stage manner. Beginning with a single axis as “active”, that is with bias signals applied, the sensor is treated as a single-axis sensor for the full characterization suite detailed above. This is followed by activating only the second axis, and repeating the measurements. A third set of measurements is then performed, with both axes active, giving particular attention to sensor system response at non-right angle orientations.

Normally incident pressure sensitivity will be a key metric in evaluating device success. The differential orientation of the comb fingers will ideally reject all common mode inputs, including pressure, but fabrication realities may complicate the issue. Furthermore, higher order resonant modes of the device structure, such as rocking modes, might generate additional instability.

Once characterization is completed the dual-axis sensor is ready for full-scale testing. Performance within the UF closed loop tunnel is compared against the single-axis devices. Calculations of correlation between the traversing hotwire and both axes of wall shear stress will help elucidate the dynamics of turbulent structures within the boundary layer. How they maintain

coherence in streamwise and crossstream directions simultaneously is of great interest. Eventually the sensor will be installed in more complex models with fully three-dimensional flow fields, opening up new sources of information which current technology cannot provide.

CONCLUSION: (500 word limit)

The development of a single-axis wall shear stress sensor for low-speed aerodynamic conditions with a capacitive transduction method has been pushed to near commercial viability. Bench top characterization indicate performance metrics matching or exceeding those previously reported. More significantly the sensor has been placed in full scale wind tunnel facilities at the home university and externally, a first in reported literature. Some minor improvements will be made, mainly to supporting packaging, which will help make the sensor available as a tool in the near future. Initial design surveys for an extension to a dual-axis solution are promising. Leveraging the work done here, a sensor prototype capable of simultaneous mean and fluctuating wall shear stress vector measurements in real time will be produced soon.